

Location dependent flight cost differences from the lunar surface to an orbital fuel depot and its influence on ISRU location selection

Sven J. Steinert^{1,*}, Paul Zabel² and Dominik Quantius²

¹ School of Engineering and Design, Technical University of Munich (TUM), Munich, Germany

² Institute of Space Systems, Systemanalyse Raumsegment, German Aerospace Center (DLR), Bremen, Germany

Correspondence*:

Sven Julius Steinert

sven.julius.steinert@outlook.com

2 ABSTRACT

With increasing relevance for lunar activities, the location selection for ISRU facilities is a necessary step to identify the most suitable configuration during mission planning. To raise information about the dominant location dependencies, a scenario was set up where an ISRU product is exported to an orbital depot and mass costs are used for classification. In the selected scenario, Oxygen is produced by an Ilmenite reduction plant and subsequently exported to the Lunar Gateway via an Oxygen-Hydrogen fueled launcher running in a round-trip, refueling Oxygen at the lunar surface and Hydrogen at the Lunar Gateway. It showed that the variations in transport costs can be either entirely avoided or have a recessive influence on the mission's total costs over an extended amount of time, such as 20 years. The identification of the top 10 most optimal locations for various resolutions were only slightly altered under consideration of flight costs compared to only considering the ISRU factors, which concludes the insignificance of flight cost dependencies for the analysed case.

Keywords: In situ resource utilization (ISRU), orbital fuel depot, delta v map, lunar outpost, location selection, Ilmenite reduction, Lunar Gateway, Near-rectilinear halo orbit (NRHO)

1 INTRODUCTION

The Moon and its currently unused resources are holding a great potential in economics and development for the human presence. The big collaborative field study of Kornuta et al. (2019) has shown, that an undertaking like this is technologically feasible which was presented in a commercial architecture. In contrast to Kornuta et al. (2019), where water ice in the permanently shadowed regions near the poles is focused as resource for Hydrogen and Oxygen via electrolysis, Oxygen could be also obtained through extraction from regolith. This involves downsides as Oxygen is only one propellant component and big machinery for regolith handling is required, but also opportunities as the abundance of Oxygen in regolith is truly vast with a combined weight percent up to 45% measured from Apollo return samples in Papike et al. (1982). This Oxygen is bonded to various elements which is where extraction methods as Hydrogen reduction of Ilmenite are focusing on one specific bond for an effective processing procedure. Therefore

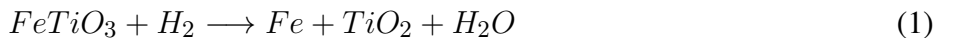
27 propellant production does not need to be restricted to the polar regions, especially when a fully robotic In
28 situ resource utilization (ISRU) plant is feasible on the lunar surface and no life support systems and their
29 water resources are required. Optimization can be therefore based on the process factors to pick the most
30 optimal location globally. For this event, the goal of this analysis is to identify the leading significance of
31 two sections of process factors, the ISRU efficiency and the transport efficiency. In case of insignificance
32 by one of these influences, a prioritization is provided for future mission analysis on similar scenarios.

2 MATERIALS AND METHODS

33 The determination of influences is approached by an example scenario under which both ISRU hardware
34 costs and flight costs can be assigned and put together into a joined model under which comparisons can be
35 drawn, through mass costs as central unit. The example scenario consists out of an ISRU Oxygen plant on
36 the lunar surface and an orbital fuel depot where a comparable launcher is delivering and consuming the
37 produced Oxygen.

38 2.1 ISRU Efficiency

39 When the optimal location is chosen by the highest ISRU efficiency, the whole production line has to be
40 inspected for location dependent factors first. Such location dependent factors are for example: raw material
41 concentration, solar irradiance, temperatures, flat surface conditions and further scenic requirements.
42 Hereby, the production method is decisive about the sensitivity to location depended factors. One prominent
43 extraction method is the Hydrogen reduction of Ilmenite which has been already demonstrated as in
44 Sargeant et al. (2020). In this process, the chemical bond of $FeTiO_3$ is broken down by Hydrogen resulting
45 in the chemical Equation 1. The resulting water is electrolyzed where the Hydrogen is fed back and the net
46 reaction leaves pure Oxygen.



47 Hydrogen reduction of Ilmenite is chosen as the production method to be analyzed, which we expect to
48 feature a high dependency on the raw material concentration and therefore a strong location dependency
49 due to inhomogeneity of Ilmenite distribution. An alternative extraction method would be molten regolith
50 electrolysis which is mostly invariant over the lunar surface, which is why all results that are derived here
51 are therefore only applicable to the chosen production method.

52 2.1.1 Model

53 To reduce model complexity, our model does include only the raw material concentration factor as
54 argument, the Ilmenite weight ratio $w_{ilmenite}$. While this does not cover all influences, the raw material
55 concentration covers a major part for the location dependency and does therefore serve as approximation
56 to a full location dependent model of Hydrogen reduction of Ilmenite. The hardware mass that has to be
57 moved to the lunar surface for ISRU operation serves as the criteria to be minimized. In a previous work of
58 (Guerrero-Gonzalez and Zabel, 2023) this hardware mass $m_{hardware}$ depending on Ilmenite concentration
59 was determined for a combined production plant of Low Carbon Steel and Oxygen production. This
60 production plant was sized for an annually output of 23.9 t Oxygen and 25 t Low Carbon Steel. The model
61 consists out of a sum of required subsystems as defined in Equation 2 (Guerrero-Gonzalez and Zabel,
62 2023).

$y_0(x) = 4036 \cdot x^{-1.064} - 9.59$	Excavation
$y_1(x) = 17580 \cdot x^{-1.003} - 390.8$	Handling
$y_2(x) = 19240 \cdot x^{-1.003} - 421.9$	Beneficiation
$y_3(x) = 21780 \cdot x^{-1.198} + 120.3$	O ₂ Extraction
$y_4(x) = 17910 \cdot x^{-1.265} + 1370$	O ₂ Purification
$y_5(x) = 29650 \cdot x^{-0.7005} - 602.5$	Metal Processing
$y_6(x) = 2541 \cdot x^{-0.7434} + 286.8$	Gas Liquefaction & Storage
$y_7(x) = 32440 \cdot x^{-0.8312} + 125.2$	Thermal Control
$y_8(x) = 12000 \cdot x^{-0.9657} + 63.99$	Power

63

$$m_{\text{hardware}}(x = w_{\text{ilmenite}} [\text{wt}\%]) = \sum_{i=0}^8 y_i(x) [\text{kg}] \quad (2)$$

64 Where in our scenario, only the Oxygen production is relevant, the additional subsystems as metal
 65 processing scale in a similar way as the rest of the system so that the spread between low and high values
 66 of w_{ilmenite} is not distorted significantly (88.69% spread to the maximum value vs. 89.97% spread without
 67 metal processing, for $1 \text{ wt}\% \leq w_{\text{ilmenite}} \leq 11 \text{ wt}\%$). Furthermore, this combined production plant could
 68 still be a viable choice out of the synergistic effects of shared infrastructure. This is why we are choosing
 69 this model to be our reference production plant as a whole rather than trimming subsystems. Therefore our
 70 model is expressed in Equation 2 as well.

71 **2.1.2 Data Processing**

72 To determine the cost for every location on the Moon, a global lunar map of Ilmenite weight ratio is
 73 required. In a previous work by Hiroyuki Sato (Sato et al., 2017) an almost global TiO₂ abundance map
 74 was created, where the values of weight percent (wt%) for TiO₂ are used as equivalent for Ilmenite. The
 75 resulting map had a mask applied to leave only lunar Mare regions and had a limited latitude coverage
 76 from -70° to 70° . The limited coverage originates from the orbiter sensor data and its limitations in
 77 measurement at an increasingly steep sunlight angle towards the poles. The initial data was created by the
 78 Lunar Reconnaissance Orbiter Camera (LROC) Wide Angle Camera (WAC) which is our starting point to
 79 recreate a similar dataset as (Sato et al., 2017) but on a global basis. The original WAC data segments are
 80 joined together in Figure 1.

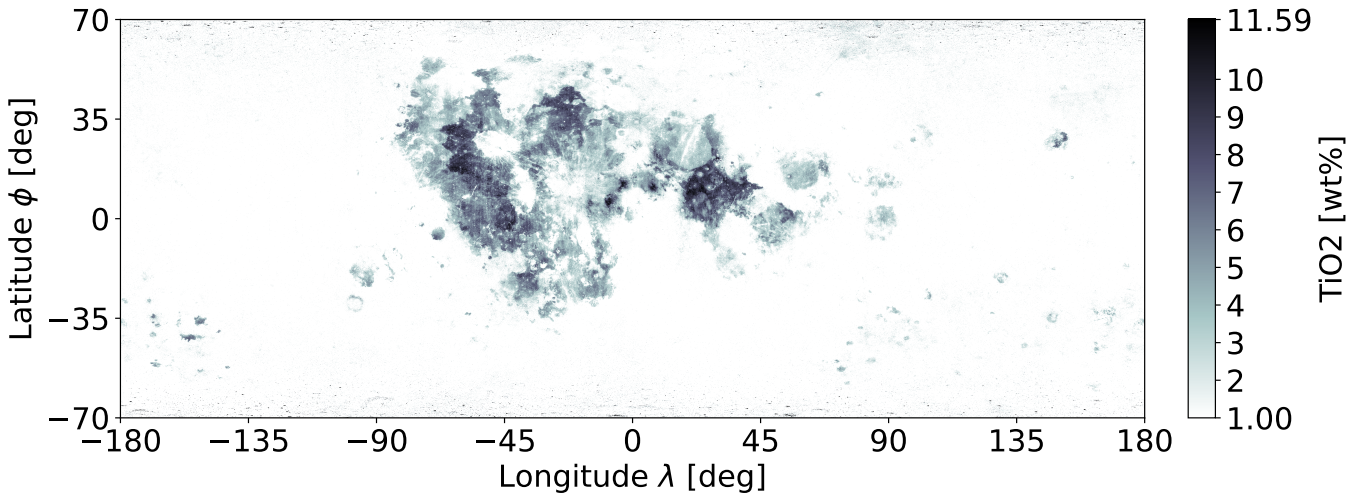


Figure 1. Combined original TiO₂ data of the WAC, (Sato et al., 2017)

81 **2.1.2.1 Cleanup and Estimation**

82 One problem are unusual high measurements towards the poles that are considered increasing noise
 83 which is scattered through the entire longitudinal axis. The second problem is the incomplete coverage of
 84 latitude and therefore the poles itself. To derive an estimation over the missing information at latitudinal
 85 coverage, the following strategy is applied. If Ilmenite abundance correlates with the classification of
 86 Highlands / Mare and the pole regions geology is featuring highland characteristics then the expected value
 87 of the known highland region serves as an estimate of Ilmenite content at the poles.

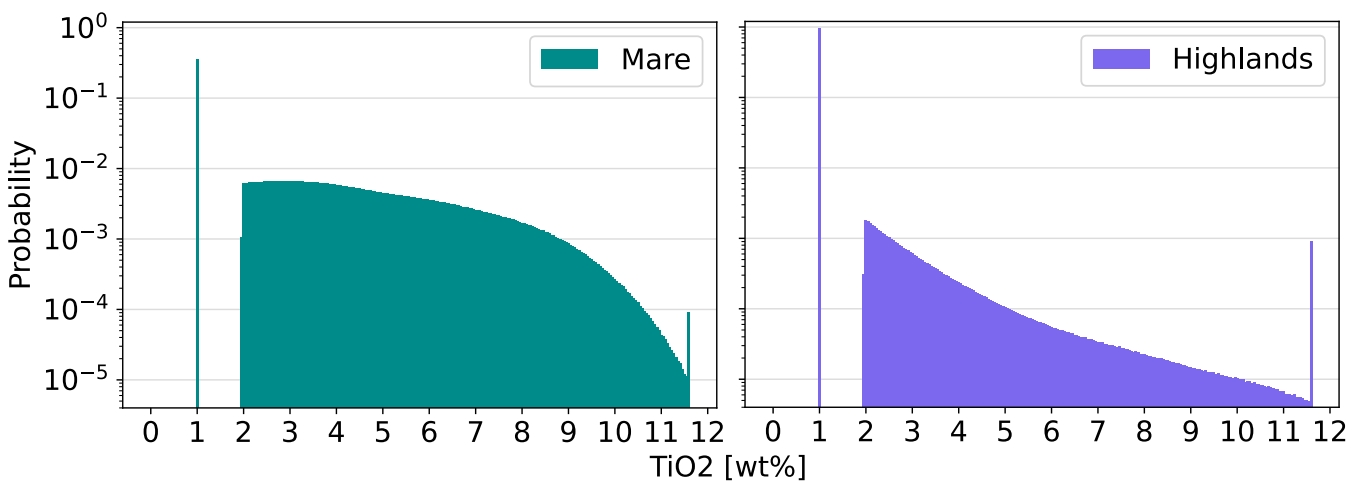


Figure 2. Distribution of Ilmenite content clustered into Highlands and Mare (equirectangular corrected) on combined WAC data with Mare boundaries from (Nelson et al., 2014)

88 As Figure 2 shows, the distribution characteristics of these two regions deviate considerably, whereby
 89 the average abundance also differs from 3.38 wt% in Mare to 1.1 wt% in Highland regions. Therefore
 90 the Ilmenite content correlation is given and the estimate over the missing latitudinal area of Highlands
 91 is set to 1 wt% which also matches the WAC original assumption for values under the detection ratio.
 92 To additionally remove the increasing noise at further extreme latitudes, a mask is created out of Mare

93 boundaries from (Nelson et al., 2014) merged with a constant separation at $\phi = \pm 56^\circ$. The replacement
 94 values for the mask are equally set to 1 wt%. With both estimates applied, a low noise global Ilmenite map
 95 is accomplished which can be seen in Figure 3.

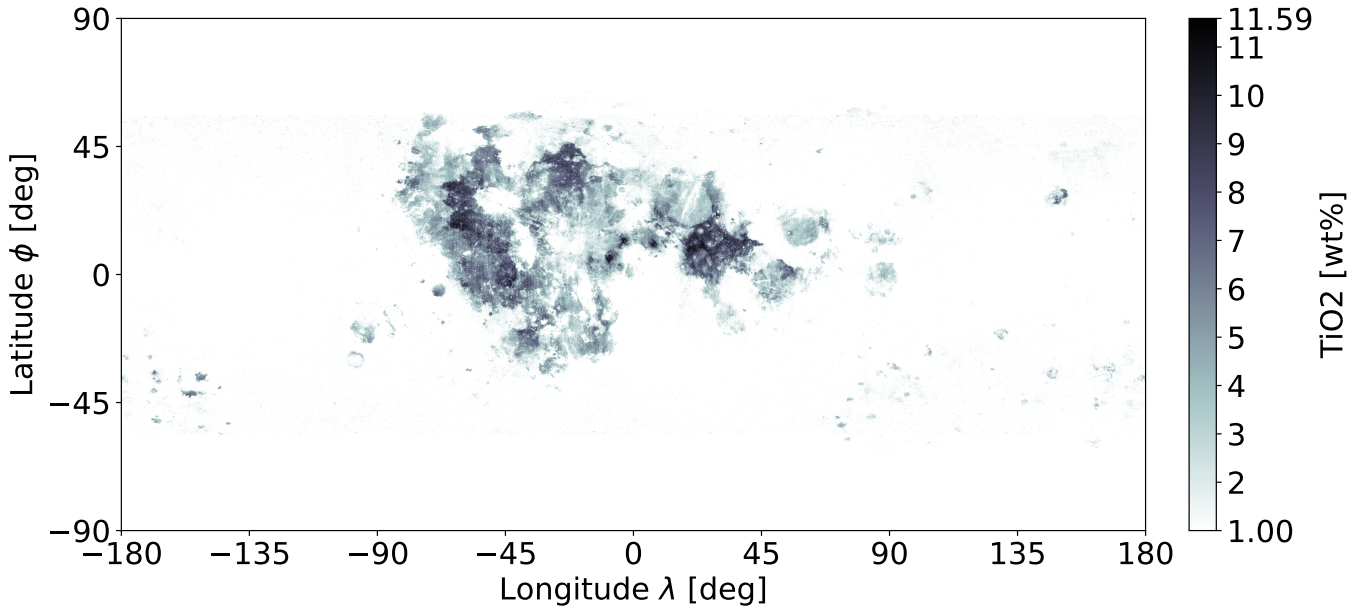


Figure 3. Global lunar Ilmenite map in weight percent through TiO_2 , based on WAC data and estimates

96 2.1.2.2 ISRU Mass Cost Map

97 This global Ilmenite abundance map from Figure 3 is now used as input to Equation 2, which is resulting
 98 in the location dependent ISRU hardware mass displayed in Figure 4.

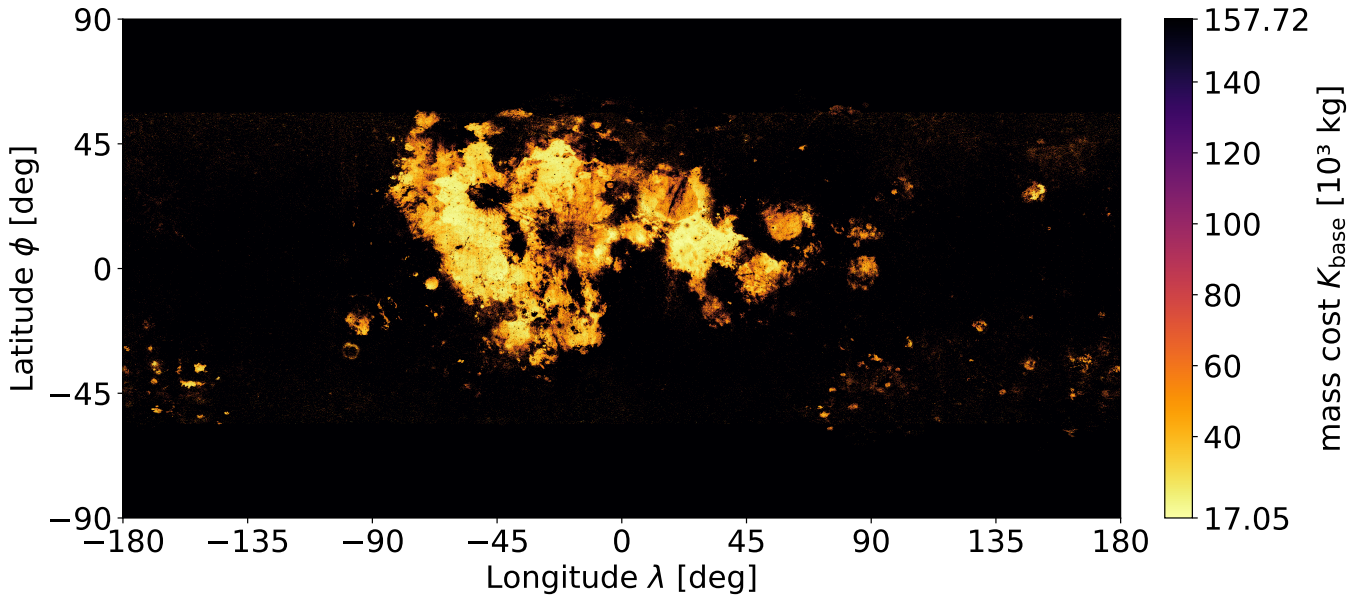


Figure 4. Location dependent ISRU hardware mass cost K_{base} in its base configuration of 23.9 t Oxygen per year

99 **2.2 Transport efficiency**100 **2.2.1 Mission Planning**

101 The mission is designed to be carried out by a single stage launcher to loop between the lunar surface
 102 and the target orbit destination. The Oxygen fuel component and the Oxygen payload are refilled on lunar
 103 ground at the ISRU production plant. The Hydrogen fuel component on the other hand is refilled at the
 104 fuel depot where also the Oxygen payload is delivered. This results effectively in an exchange of delivered
 105 Oxygen to deducted Hydrogen from the station. A multi staged launcher or a shuttle exchange system was
 106 neglected for this analysis but would hold the potential to further increase the transport efficiency.

107 **2.2.2 Orbital Fuel Depot Location**

108 The primary requirement of the fuel depot location is its accessibility from both the supplying and
 109 consuming units. For an interplanetary or cis-lunar logistic hub near Earth, Liberation points are especially
 110 suited as considered by previous studies from Perrin and Casler (2016). Similar to Liberation points, their
 111 corresponding halo orbits are offering the benefits of accessibility as well. In the case for an interplanetary
 112 logistic hub near Earth which is supplied by the lunar surface, the currently planned Lunar Gateway on its
 113 Near-rectilinear halo orbit (NRHO) fits prodigiously as a theoretical test bed for this purpose. Additionally,
 114 a NRHO fuel depot was also considered in the commercial lunar propellant export study by Kornuta et al.
 115 (2019). Which is why the Lunar Gateway orbit is chosen to be analysed in this scenario as the export
 116 destination and considered a fuel depot.

117 **2.2.3 Target Orbit**

118 For the selected fuel depot location at the Lunar Gateway, the target orbit is a specific NRHO that is in a
 119 9:2 Lunar Synodic Resonance with an average perilune of $h_{peri} = 3557 \text{ km}$ and an average orbital period
 120 of $T = 6.562 \text{ days}$ (Lee, 2019). It is worth mentioning that this orbit has a varying polar crossing as well
 121 as other time dependent changes in its trajectory which are often simplified to more static conditions for
 122 analysis (Whitley et al., 2018).

123 **2.2.4 Delta-v Estimation**

124 First of all, regardless of the mission or the trajectory, planetary conditions such as ground elevation and
 125 surface velocity are influencing the required Δv . These influences are now briefly assessed for the Moon to
 126 determine their relevance.

127 **2.2.4.1 Celestial Influences**

128 The initial radial distance to the Moon's center of mass $r(\phi, \lambda)$ influences the ideal Δv demand directly
 129 as shown for an ascent into a circular orbit at r_{orbit} in Equation 3.

$$\Delta v_{ideal}(\phi, \lambda) = \sqrt{v_{orbit}^2 + v_{ascent}^2} = \sqrt{\left(\frac{\mu}{r_{orbit}}\right) + \left(2 \cdot g_0 \cdot \left[r(\phi, \lambda) - \frac{r(\phi, \lambda)^2}{r_{orbit}}\right]\right)} \quad (3)$$

130 Global ground elevation data is now used in the form of a displacement map (Ernie Wright and Noah
 131 Petro, 2019), which originates on Lunar Orbiter Laser Altimeter (LOLA) measurements (David E. Smith,
 132 2015). The elevation ranges from -9.115 km to 10.757 km with regard to the reference radius r_{ref} of 1737.4
 133 km and therefore defines $r(\phi, \lambda)$ globally. The displacement map is shown in Figure 5.

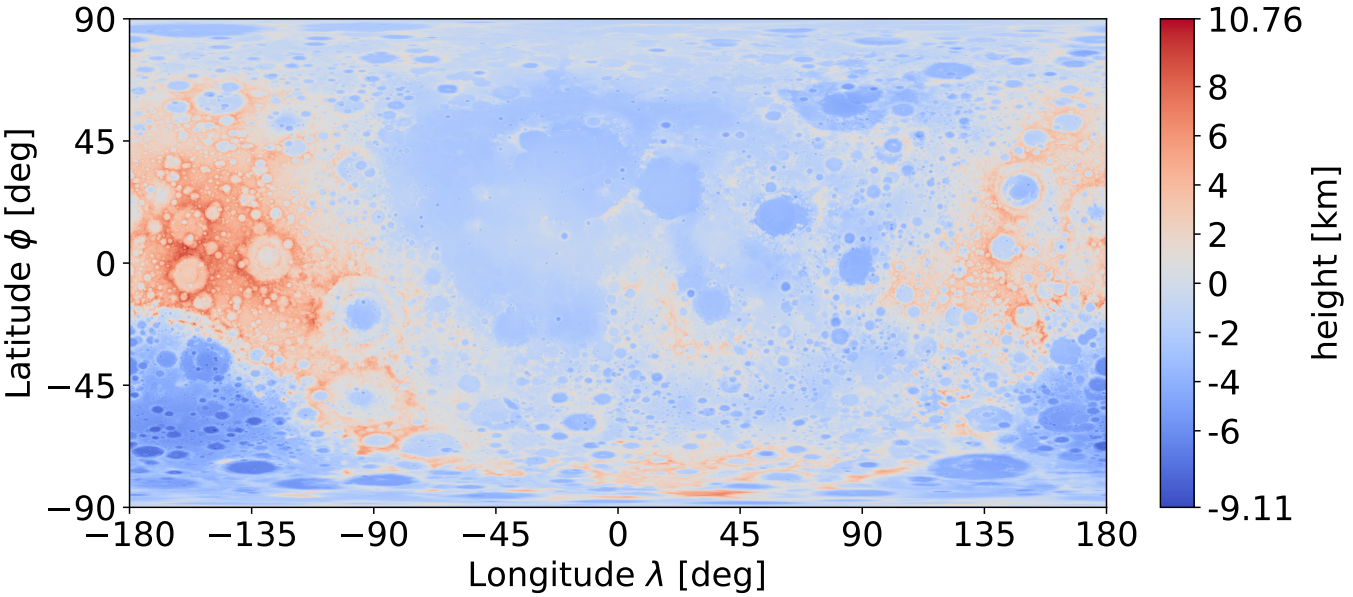


Figure 5. Lunar displacement map to reference radius ($r_{\text{ref}} = 1737.4 \text{ km}$). Data from NASA CGI Kit (Ernie Wright and Noah Petro, 2019) based on (David E. Smith, 2015)

Evaluating the extreme values on a Low Lunar Orbit (LLO) at 100 km altitude ($r_{\text{orbit}} = 1837.4 \text{ km}$) with Equation 3 yields:

$$\begin{aligned}\Delta v_{\min} &= \Delta v_{\text{ideal}}(\max \{r(\phi, \lambda)\}) = 1725.187 \frac{\text{m}}{\text{s}} \\ \Delta v_{\max} &= \Delta v_{\text{ideal}}(\min \{r(\phi, \lambda)\}) = 1725.204 \frac{\text{m}}{\text{s}}\end{aligned}$$

- 134 The influence on Δv from ground elevation is therefore at the order of 0.001 % which is extremely low.
 135 The second celestial influence, the initial surface velocity v_0 is either an additional Δv demand or a Δv
 136 reduction, depending on the shared velocity components to the launch direction. Together with the sidereal
 137 rotation period and the assumption of a spherical lunar surface of r_{ref} , the surface velocity can be given as
 138 a function of Latitude ϕ as displayed in Equation 4.

$$v_0(\phi) = \frac{2\pi}{27.322 \text{ days}} \cdot \cos(\phi) \cdot r_{\text{ref}} \quad (4)$$

- 139 Evaluating the extreme points of polar and equatorial locations on Equation 4 yields:

$$\begin{aligned}\Delta v_{\min} &= \Delta v_0(\phi = \pm 90^\circ) = 0.000 \frac{\text{m}}{\text{s}} \\ \Delta v_{\max} &= \Delta v_0(\phi = 0^\circ) = \pm 4.624 \frac{\text{m}}{\text{s}}\end{aligned}$$

- 140 Comparing this range $|\Delta v_{\max}| - \Delta v_{\min}$ to the ascent from the reference radius to a circular 100 km
 141 LLO being $\Delta v_{\text{ideal}}(r_{\text{ref}}) = 1725.196 \frac{\text{m}}{\text{s}}$ gives the Δv influence of the surface velocity to be at the order
 142 of 0.27 % which is significantly more than the elevation influences but still considerably low.

143 2.2.4.2 Transfer Options

- 144 Explicit Transfers from any lunar geodetic point to NRHOs and vice versa are a high-fidelity problem
 145 which is usually solved non-analytically as in (Trofimov et al., 2020). Additionally, there are multiple

146 transfer strategies that can be deployed for different optimisation goals. Between optimisation of required
 147 Δv and transfer time, two transfer options are being analysed for our chosen scenario.

148 First, a long duration transfer that features a very low required Δv of only $664.9 \frac{m}{s}$ to a LLO at 100
 149 km altitude, which is very close to the theoretical limit of $654.8 \frac{m}{s}$ as minimum energy change (Whitley
 150 et al., 2018). Also, it features an almost complete independency to surface location, which is reached
 151 by something similar to a Three-Impulse transfer, where the lunar sphere of influence is left to circle
 152 once around Earth before inserting again. This allows any inclination restrictions to vanish, but at a cost
 153 of a 100.1 day long transfer time. If this transfer option is chosen, the influence of transfer efficiency
 154 is extremely low and marginal to the ISRU dependencies derived in Chapter 2.1. In this case transfer
 155 dependencies can be neglected and the location selection can be simplified to only ISRU efficiency.

156 Often however a 100 day transfer time is simply too long for certain applications, as it for example induces
 157 general system lag time and therefore poor dynamics in propellant delivery adjustments in the case of the
 158 subjected mission. For this reason, a second transfer option is analysed which is a direct transfer trajectory
 159 between the NRHO and the surface from Trofimov et al. (2020), which features the shortest transfer time
 160 of only hours but at the cost of higher Δv and location dependency. The direct transfer, illustrated in Figure
 161 6, is the subject of the following analysis in the following sub-chapters.

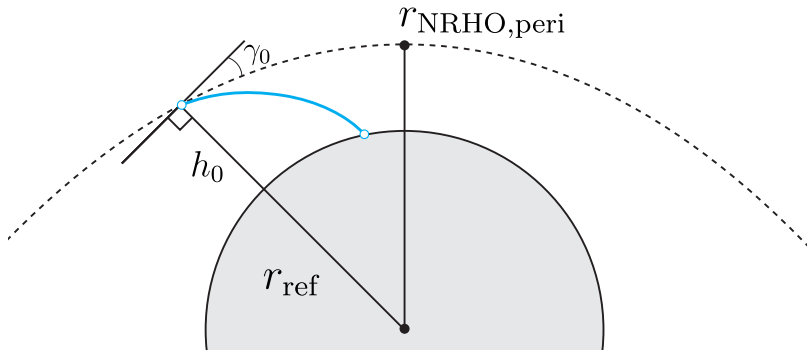


Figure 6. Direct ascent trajectory scheme via gravity turn, according to Trofimov et al. (2020)

162 2.2.4.3 Data Processing

163 In the previous work by Trofimov et al. (2020), a set of possible direct decent trajectories and their
 164 associated landing point and Δv demand were identified. The resulting map of scatter points for the
 165 southern 9:2 NRHO was taken as starting point to derive a global Δv map. Since always the cheapest
 166 option for one location would be chosen, a minimum estimation was performed. This estimation was
 167 done by splitting the map into 20 deg square tiles where constancy is assumed and the lowest value is set
 168 for the whole tile. In preparation for this, the data has been cut from particular high costs trajectories of
 169 $\Delta v > 2985.65 \frac{m}{s}$ due to rather leaving non defined tiles at the poles than carrying up to $3300 \frac{m}{s}$ transfer
 170 options over into the final map. This process is visualized in Figure 7.

171 The non defined tiles have been linear interpolated along the longitudinal axis, which was only necessary
 172 in polar regions where there is already a higher geodetic resolution due to equirectangular projection. This
 173 leads to our final Δv map, depicted in Figure 8.

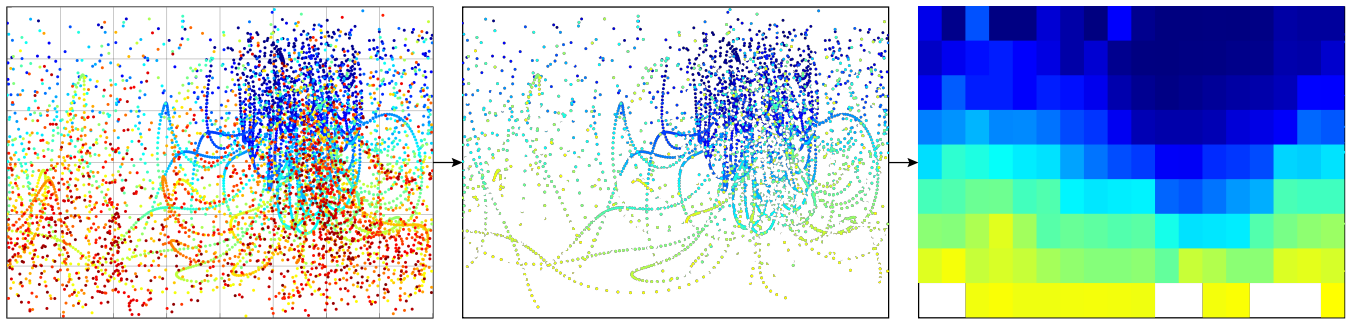


Figure 7. Processing of results from Trofimov et al. (2020) (left) to cutting of data (center) into minimum of 20 deg square tiles (right)

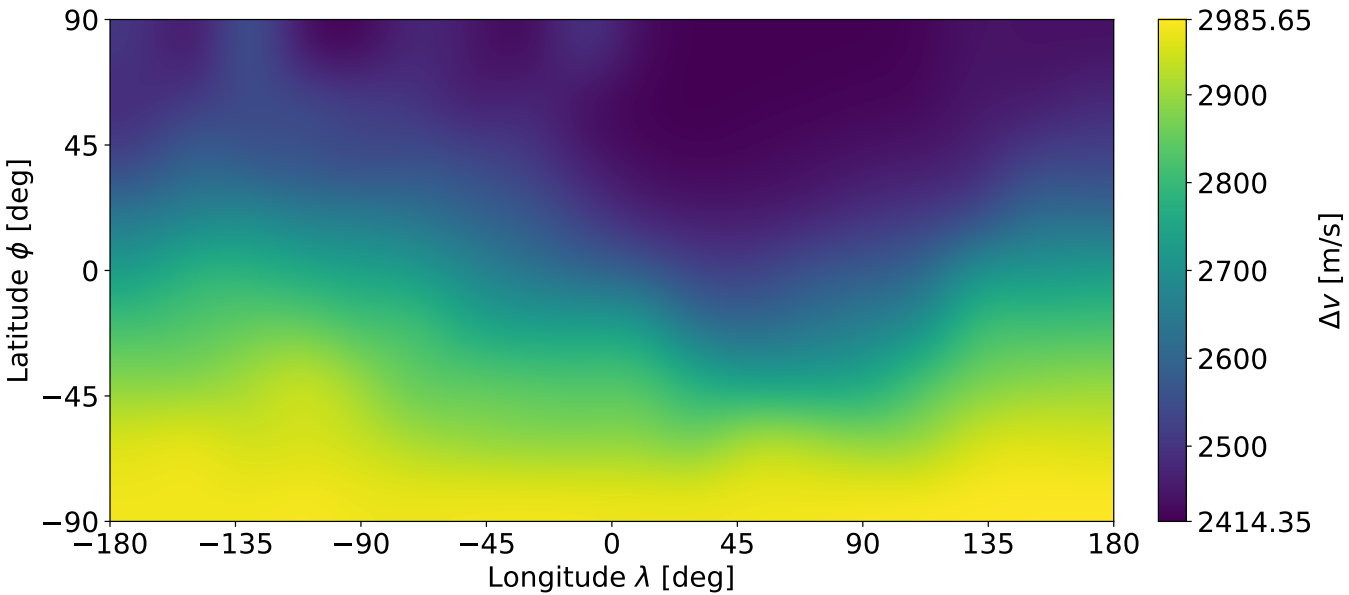


Figure 8. Required Δv for direct decent from southern 9:2 NRHO to the lunar surface (bicubic interpolated)

174 2.2.4.4 Delta v Map

175 Even though this data was computed for the decent only, it will serve as estimation for the ascent as well,
 176 which is holding a bias as those problems are not entirely symmetric. Additionally, it should be mentioned
 177 that even though a $2414 \frac{m}{s}$ transfer is very viable, a transfer of around $2900 \frac{m}{s}$ might be rather replaced in
 178 a real world scenario by a different transfer strategy, as via a LLO with waiting time to save Δv . However
 179 in this analysis, Figure 8 defines $\Delta v(\phi, \lambda)$ globally with $\Delta v_{min} = 2414.35 \frac{m}{s}$ and $\Delta v_{max} = 2985.65 \frac{m}{s}$.

180 2.2.5 Transport Carrier

181 2.2.5.1 Reference Launcher

182 To derive associated transport mass costs, the previously determined Δv has to be applied on a specific
 183 launcher. The Argonaut, formerly known as the European Large Logistics Lander (EL3), is chosen as
 184 a starting point for this scenario. The initial configuration is based on the time of writing published
 185 information from the European Space Agency (2023) of 10 000 kg wet mass, 1600 kg dry mass and 2100
 186 kg payload. Additionally a Hydrogen (H₂), Oxygen (O₂) propulsion system with an oxidizer fuel ratio of 6

187 and 400 s of specific impulse are assumed. When this original configuration is applied on our mission with
 188 Δv_{max} the fuel is running out before the round-trip can be completed. Therefore the launcher configuration
 189 has to be altered for our scenario needs.

190 2.2.5.2 Launcher Up-scaling

191 An up-scaling is performed, where the dry mass is kept constant at 1600 kg but fuel is added until
 192 the mission can be completed. The minimal viable system features an empty H₂ tank at arrival at the
 193 Gateway and an empty O₂ tank at the lunar surface. The Iteration scheme of the up-scaling is visualized in
 194 Figure 9 which can now converge a minimal viable launcher for any given payload. Hereby describes "H₂
 195 insufficient" the failure case when the launcher returned but does not have enough H₂ to do the next run.

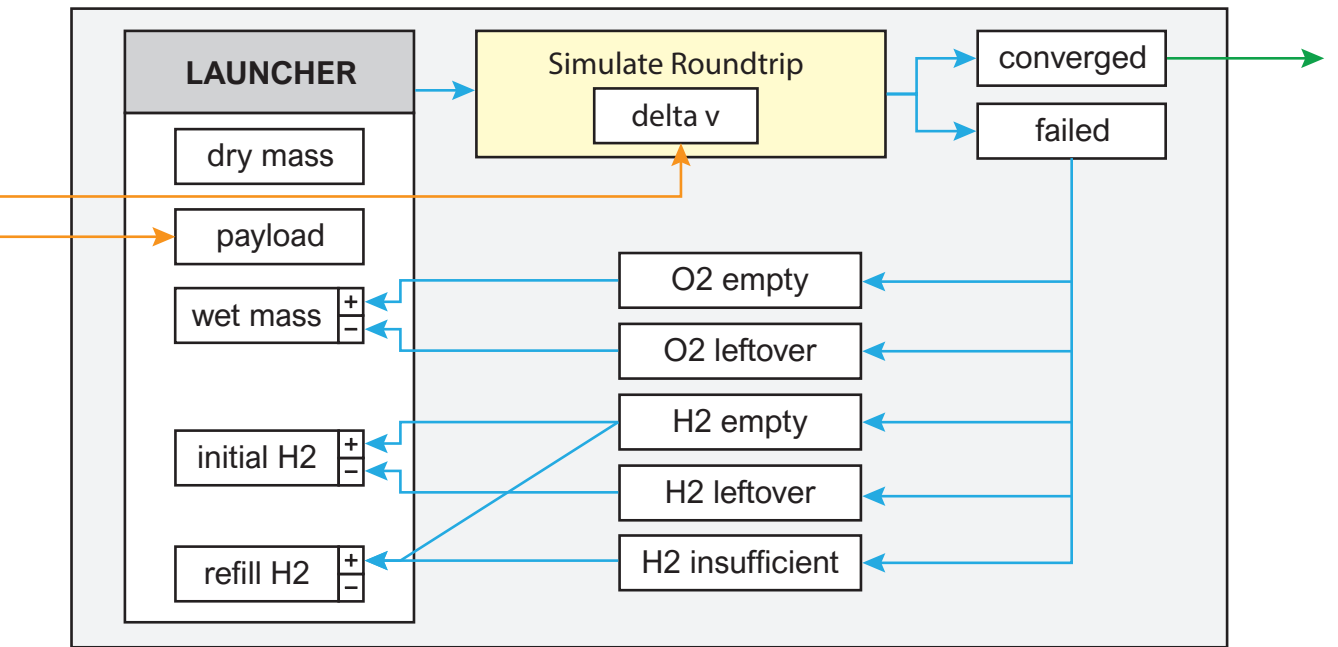


Figure 9. Launcher iteration scheme to converge a roundtrip for a given payload and Δv

196 Since this method of up-scaling is effectively increasing the mass ratio ($r_m = \frac{m_{wet}}{m_{dry}}$) of the launcher, this
 197 assumption becomes increasingly unrealistic. Additionally, from the perspective of the fuel depot, Oxygen
 198 is delivered but also Hydrogen is taken away, therefore effectively trading those masses by the exchange
 199 ratio ($r_{ex} = \frac{m_{payload}}{m_{H2,refill}}$). In order to bring a decision to what range of launchers shall be compared to derive
 200 cost differences, Figure 10 visualises the parameter space between the exchange ratio r_{ex} and the mass
 201 ratio of the launcher r_m .

202 Hereby there are two sections grayed out, once $r_{ex} < 1$ out of economic reasonableness and second
 203 $r_m > 10$ as a soft border of mass ratios for realistic single stage launchers. The selection of the chosen
 204 launcher frames was done through a sequence of movements in the parameter space. Starting by the
 205 economical reasonable exchange ratios of 1.5 and 2.0 (solid black lines, also called milestones), which
 206 is then projected to their required mass ratio (dashed black line). This currently holds a set of constant
 207 exchange ratio throughout the Δv range, in order to obtain comparable results however, the mass ratio r_m
 208 has to be constant over one set as it represents the efficiency of the launcher. Therefore, the maximum
 209 value of the mass ratio (at Δv_{max}) is set as constant over the Δv range which is then yielding the chosen

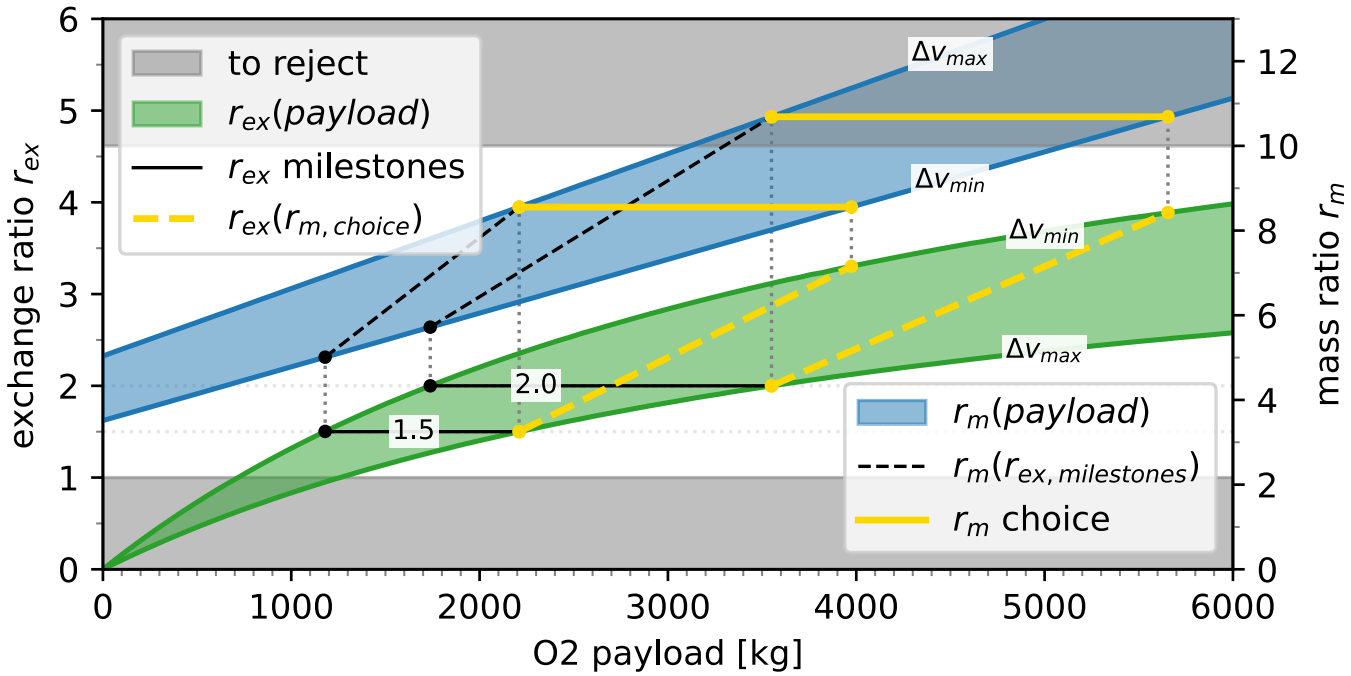


Figure 10. Exchange ratio r_{ex} and mass ratio r_m depending on payload size of the launcher over Δv range

210 frame regarding the mass ratio (solid yellow line). When this set is then projected back onto the exchange
211 ratio (yellow dashed line), a span of exchange ratios is featured over the Δv range.

212 This concludes the two chosen frames (yellow lines) of:

$$r_m = 8.555 \text{ with } 1.5 \leq r_{ex} \leq 3.303$$

$$r_m = 10.688 \text{ with } 2.0 \leq r_{ex} \leq 3.889$$

213 To analyse the problem on two frames of different mass ratios is providing insight on the sensitivity
214 towards more efficient launchers in general and their influence on the location selection.

215 **2.2.5.3 Spent Fuel**

216 Through another iteration scheme, which is targeting the chosen mass ratio r_m , a launcher can be
 217 converged for any Δv . The expended fuel is directly drawn from the simulated round-trip and normalized
 218 by the payload size, which therefore can be combined into a direct mapping from required Δv to the spent
 219 fuel k_{Flight} in kg per kg payload. This dependency can be seen in Figure 11 for both chosen mass ratios
 220 $r_m = 8.6$ and $r_m = 10.7$. In this comparison, the higher mass ratio $r_m = 10.7$ features a smaller absolute
 221 and relative growth, which concludes that differences in spent fuel decrease in general by an increasing
 222 launcher efficiency.

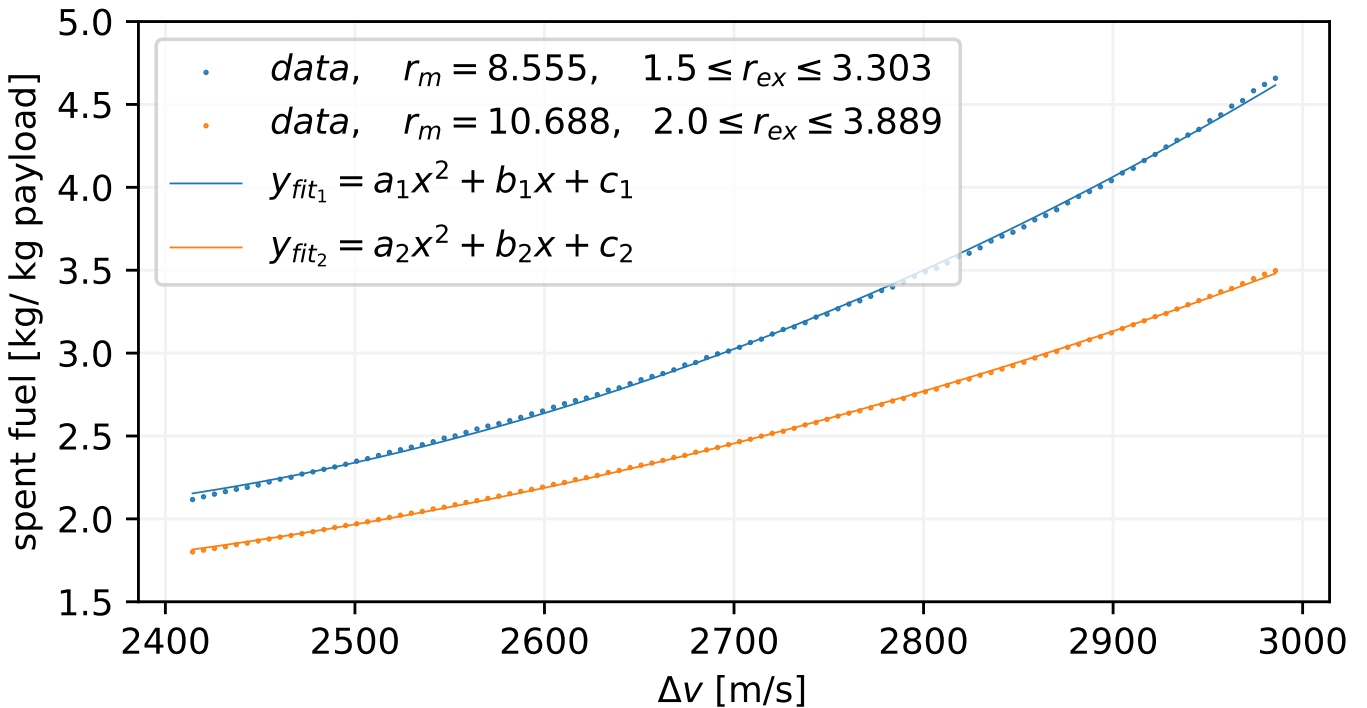


Figure 11. Relationship between required Δv and spent fuel k_{Flight} for both mass ratios

223 2.3 Joined Model

224 2.3.1 Total Cost Modelling

225 When both influences from Section 2.1 and Section 2.2 are combined, the comparable mass costs have to
 226 be drawn from the mission scenario. Rather than assuming all expended fuel as transport cost, a separation
 227 of the fuel components is done, due to the reason that the Oxygen is not being shipped from Earth but
 228 rather fully supplied by the ISRU facility.

229 2.3.1.1 Fix Costs

230 In order to meet the additional demand of Oxygen per year, that the launcher requires for transport,
 231 the ISRU facility is scaled up linearly by its ISRU costs per kg Oxygen k_{ISRU} for each location and its
 232 corresponding fuel requirements. The scaling factor originates from the base configuration costs from
 233 Figure 4 and its annual base production $m_{\text{base}} = 23.9 \text{ t}$, which gives: $k_{\text{ISRU}}(\phi, \lambda) = \frac{K_{\text{base}}(\phi, \lambda)}{m_{\text{base}}}$. The
 234 additional Oxygen demand per year is derived by the yearly payload $m_{\text{pl,y}} = 8 \text{ t}$, which has been set to
 235 minimize scaling on the base configuration, the oxidiser-fuel-ratio r_{of} and the spent fuel k_{Flight} depending
 236 on the two selected mass ratios $r_m \in \{8.6, 10.7\}$. Therefore the fix costs, which represent the Earth
 237 supplied mass for the construction of the ISRU facility are:

$$238 K_{\text{Fix}}(\phi, \lambda, r_m) = K_{\text{base}}(\phi, \lambda) + k_{\text{ISRU}}(\phi, \lambda) \left(\left[m_{\text{pl,y}} \cdot k_{\text{Flight}}(\phi, \lambda, r_m) \cdot \frac{r_{\text{of}}}{r_{\text{of}} + 1} \right] + m_{\text{year}} - m_{\text{base}} \right) \quad (5)$$

238 2.3.1.2 Dynamic Costs

239 The expended Hydrogen is considered fully as mass cost since it is taken from the Lunar Gateway depot
 240 and assumed to be delivered by Earth. Hereby the cost level of the Lunar Gateway and the lunar surface
 241 are simplified as equal from Earth to be comparable, which rather overestimates the Hydrogen's cost in
 242 comparison to costs on the lunar surface when supplied from Earth. Therefore the dynamic costs, which
 243 represent the Earth supplied mass for Hydrogen on the Lunar Gateway per year t are:

$$244 K_{\text{Dynamic}}(\phi, \lambda, t, r_m) = t \cdot m_{\text{pl,y}} \cdot k_{\text{Flight}}(\phi, \lambda, r_m) \cdot \frac{1}{r_{\text{of}} + 1} \quad (6)$$

244 2.3.1.3 Total Costs

245 Combining both K_{Fix} and K_{Dynamic} , the final total costs of the mission over location and time are:

$$246 K_{\text{Total}}(\phi, \lambda, t, r_m) = K_{\text{Fix}}(\phi, \lambda, r_m) + K_{\text{Dynamic}}(\phi, \lambda, t, r_m) \quad (7)$$

246 Applying Equation 7 with location dependent results from Section 2.1.2.2 and Section 2.2.5.3 gives the
 247 total cost maps for the mission time of 20 years for $r_m = 8.6$ in Figure 12 and $r_m = 10.7$ in Figure 13.

248 In the direct comparison between Figure 12 and Figure 13, the flight cost influence is visibly less
 249 pronounced for the increased mass ratio. Also, a reduced variation in total mission cost can be observed.

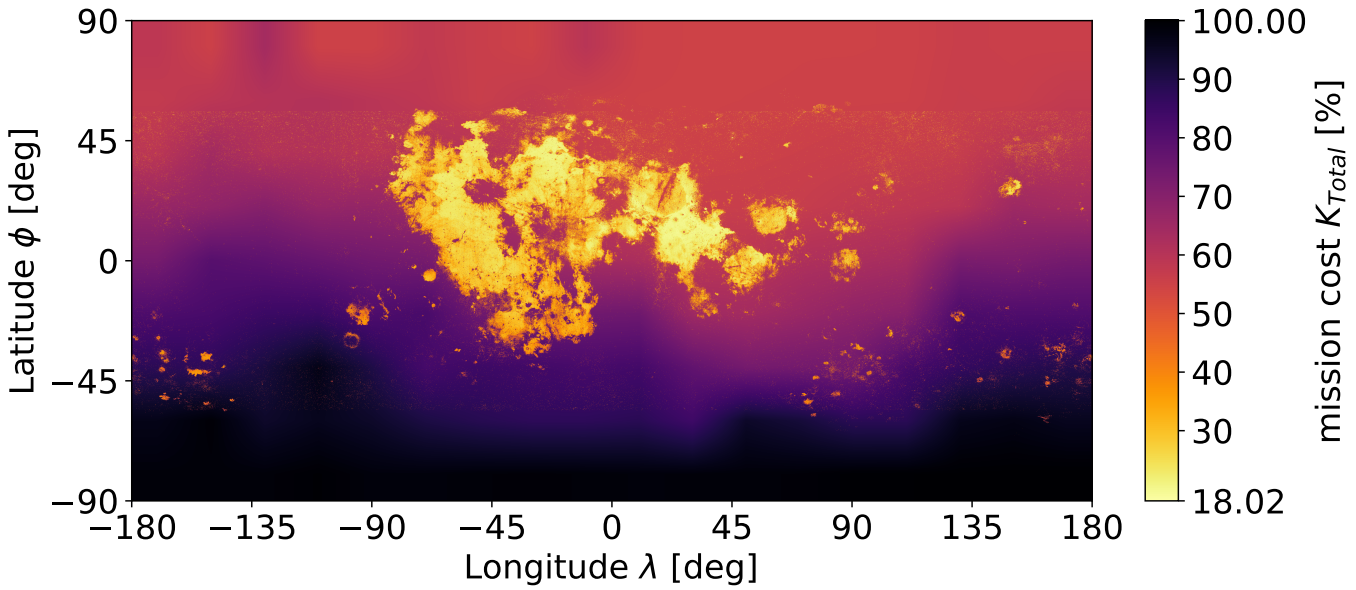


Figure 12. Location dependent total mission cost K_{Total} in % with $t = 20$ years and $r_m = 8.6$

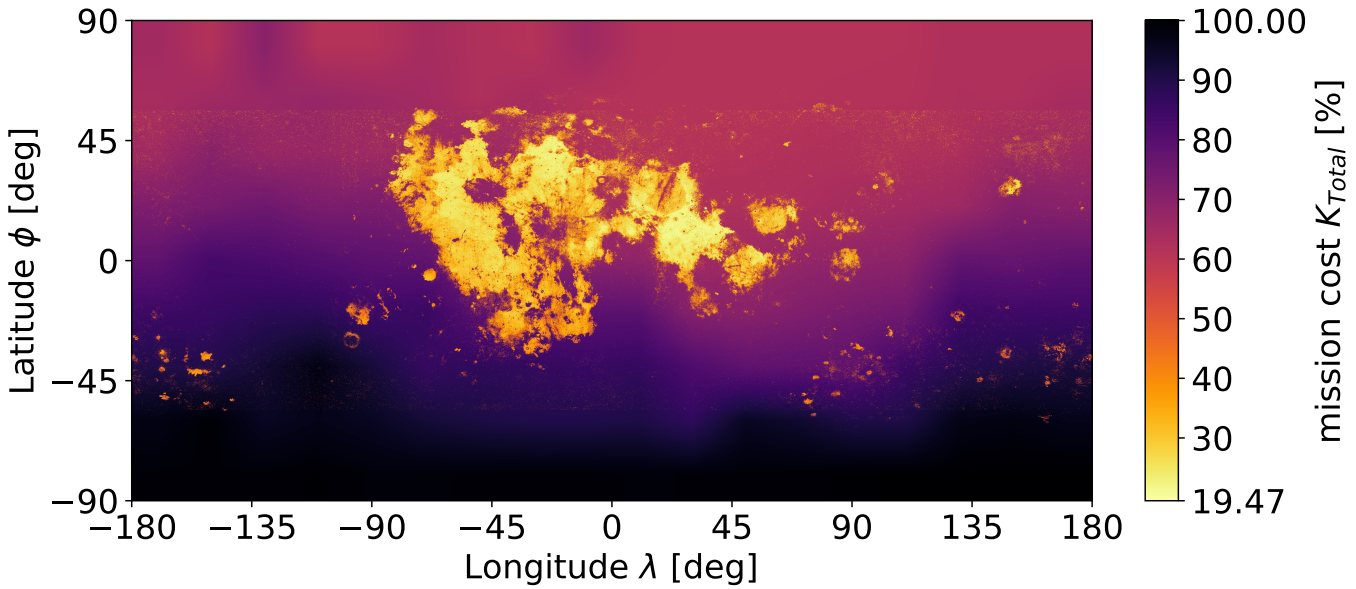


Figure 13. Location dependent total mission cost K_{Total} in % with $t = 20$ years and $r_m = 10.7$

3 RESULTS

250 3.1 Flight Cost Influences

251 In the case of the availability of the long duration transfer (Section 2.2.4.2) which is able to diminish
 252 location dependencies almost completely, as well as insignificant celestial influences (Section 2.2.4.1), the
 253 effects on the missions location selection are eliminated by an assumable uniform Δv requirement.

254 Only under the short duration transfer strategy of a direct ascent, location dependent Δv requirements
 255 are prominent (Section 2.2.4.4) which translate to a significant difference in spent fuel (Section 2.2.5.3).
 256 On the other side at the ISRU influence, Ilmenite reduction introduces vast location dependencies (Section

257 2.1.2.2), which overshadow the differences in the spent fuel, resulting in an ISRU feature dominated total
 258 cost when both influences are combined (Section 2.3.1.3).

259 3.2 Flight Cost Insignificance

260 To provide insight on the induced error when the flight costs are neglected completely, the best locations
 261 from the ISRU model from Section 2.1 are compared to the best locations from the Joined model from
 262 Section 2.3. In order to limit the possible locations, both models location dependent results are reduced
 263 into geodetic square tiles of 15° , 5° and $1^\circ(\phi, \lambda)$, to compare the behaviour on multiple resolutions. The
 264 creation of the tiles $T_{\phi \text{ index}, \lambda \text{ index}}$ was performed considering pixel area relation and yields an index
 265 resolution of 12×24 , 36×72 and 180×360 . From the created tiles, the top 10 choices are ranked and
 266 compared over the models. The top 10 choices make up the top 3.47 % for the 15° tiles, the top 0.39 %
 267 for the 5° tiles and the top 0.015 % for the 1° tiles. In Table 1, the tiles are colorized by the ranking of
 268 the ISRU model, from green as most optimal to orange as less optimal locations, giving the baseline for
 269 comparison of ordering and featured tiles. Underneath the Joined model is shown in tree time steps, at 0,
 270 10 and 20 years, providing a sense of temporal evolution of the featured tiles.

15° tiles	#1	#2	#3	#4	#5	#6	#7	#8	#9	#10
ISRU	$T_{5,8}$	$T_{5,13}$	$T_{3,10}$	$T_{4,7}$	$T_{6,9}$	$T_{3,8}$	$T_{5,14}$	$T_{4,13}$	$T_{6,8}$	$T_{4,10}$
J. t = 0	$T_{5,8}$	$T_{5,13}$	$T_{3,10}$	$T_{4,7}$	$T_{3,8}$	$T_{4,13}$	$T_{5,14}$	$T_{6,9}$	$T_{4,10}$	$T_{5,11}$
J. t = 10	$T_{5,13}$	$T_{3,10}$	$T_{5,8}$	$T_{4,13}$	$T_{4,7}$	$T_{3,8}$	$T_{5,14}$	$T_{6,9}$	$T_{4,10}$	$T_{5,11}$
J. t = 20	$T_{5,13}$	$T_{3,10}$	$T_{5,8}$	$T_{4,13}$	$T_{5,14}$	$T_{3,8}$	$T_{4,7}$	$T_{4,10}$	$T_{4,12}$	$T_{5,11}$
5° tiles	#1	#2	#3	#4	#5	#6	#7	#8	#9	#10
ISRU	$T_{15,40}$	$T_{14,24}$	$T_{16,41}$	$T_{14,23}$	$T_{16,40}$	$T_{12,23}$	$T_{10,31}$	$T_{13,24}$	$T_{15,25}$	$T_{15,42}$
J. t = 0	$T_{15,40}$	$T_{16,41}$	$T_{16,40}$	$T_{14,24}$	$T_{10,31}$	$T_{15,42}$	$T_{15,43}$	$T_{14,23}$	$T_{15,41}$	$T_{16,42}$
J. t = 10	$T_{15,40}$	$T_{16,41}$	$T_{16,40}$	$T_{15,42}$	$T_{10,31}$	$T_{15,43}$	$T_{15,41}$	$T_{16,42}$	$T_{17,40}$	$T_{11,31}$
J. t = 20	$T_{15,40}$	$T_{16,41}$	$T_{15,42}$	$T_{15,43}$	$T_{16,40}$	$T_{10,31}$	$T_{15,41}$	$T_{16,42}$	$T_{11,31}$	$T_{14,41}$
1° tiles	#1	#2	#3	#4	#5	#6	#7	#8	#9	#10
ISRU	$T_{79,204}$	$T_{81,201}$	$T_{80,200}$	$T_{72,118}$	$T_{80,201}$	$T_{84,171}$	$T_{72,117}$	$T_{81,199}$	$T_{72,116}$	$T_{80,204}$
J. t = 0	$T_{79,204}$	$T_{81,201}$	$T_{80,200}$	$T_{80,201}$	$T_{80,204}$	$T_{81,199}$	$T_{80,203}$	$T_{79,203}$	$T_{80,199}$	$T_{81,200}$
J. t = 10	$T_{79,204}$	$T_{80,200}$	$T_{80,201}$	$T_{81,201}$	$T_{80,204}$	$T_{79,203}$	$T_{80,203}$	$T_{76,201}$	$T_{78,218}$	$T_{78,204}$
J. t = 20	$T_{79,204}$	$T_{71,206}$	$T_{78,218}$	$T_{76,201}$	$T_{75,206}$	$T_{77,212}$	$T_{76,206}$	$T_{80,204}$	$T_{80,201}$	$T_{79,203}$

Table 1. Top 10 best mission locations compared between ISRU model and Joined model (J.) after t years in pixel area relation resized square tiles ($\tilde{T}_{\phi \text{ index}, \lambda \text{ index}}$) with resolution ϕ, λ of 15° (top), 5° (middle) and 1° (bottom). Indices starting at zero on $(90^\circ\phi, -180^\circ\lambda)$ with -180° to 180° Longitude range. Data from mass ratio $r_m = 8.6$.

271 The induced error of the flight cost neglect increases over mission time, but nevertheless even at greater
 272 time spans as 20 years, the top 10 of the Joined model are featuring many tiles which have been in the
 273 top 10 of the ISRU ranking. The increased conservation of the highest ranked tiles can be explained
 274 by the coincidental overlap of low flight costs and low ISRU costs. In higher resolutions less tiles are
 275 shared, however due to the difference in percentage the top 10 make up for the whole set, the shared tiles
 276 are remaining substantial. Therefore, from Table 1 is concluded that the induced error during location
 277 selection is found to be small enough that a simplification, to only consider the ISRU effects, appears a
 278 valid approximation even for greater differences in Δv as in the analysed case.

4 DISCUSSION

279 The identification of the secondary relevance and even neglect of flight costs in the selected mission
280 scenario can not directly be generalized without requirements, as for other ISRU production methods,
281 target orbits, trajectories or mass ratios each of their influence can differ greatly from the analysed case.

282 However, under the given case of Ilmenite reduction and transport properties that are comparable or
283 weaker than the analysed case, flight costs differences can be assumed insignificant. In particular, the
284 major influence to verify in a quick assessment of a general case is the estimation of differences in Δv
285 requirements, which should be less than the analysed case of $\approx 20\%$. Lower mass ratios of the launcher
286 are amplifying these differences in Δv when transferred to spent fuel and therefore fuel costs. Furthermore
287 should be mentioned that this analysis featured a scenario which involved propellant refilling by own
288 entities which reduces the fuel costs in general, which needs to be considered when other cost modelling is
289 present. Additionally, the flight frequency is scaling up flight costs linearly and can compress the shift over
290 time for the most optimal location, where as a rough reference value the delivered payload of 8 t per year
291 can be considered from the analysed case.

292 Although a significant difference in the accessibility of the southern hemisphere was the result of the direct
293 ascent trajectory, it needs to be underlined that this does not conclude a worse accessibility from the NRHO
294 to the southern hemisphere in general. In the chosen set of trajectories no options for intermediate parking
295 orbits are considered, which however if considered would bring these differences between northern and
296 southern hemisphere down, as the 1 day transfer in May et al. (2020) shows entirely different characteristics.

297 As global lunar data is increasingly present, problems as these can be analysed and optimised close to
298 their entirety over the whole lunar surface. Especially in the current stage of time where no infrastructure is
299 yet deployed on the lunar surface, location selection can be carried by optimisation instead of dependencies
300 by prior infrastructure.

301 To not create a prior infrastructure restriction ourselves, the plan for man-kinds presence and economics
302 and even sustainability on the Moon should be expanded and seen in a bigger scope as much as possible.
303 As this Oxygen propellant facility is just one entity of an economics network, which might move its most
304 optimal location completely away in bigger context from its individually analysed location. Such a large
305 scale technical investigation would make for a compelling future study.

CONFLICT OF INTEREST STATEMENT

306 The authors declare hereby that the research was conducted in the absence of any commercial or financial
307 relationships that could be construed as a potential conflict of interest.

AUTHOR CONTRIBUTIONS

308 SS conducted the research, created the solution methods and wrote the paper. PZ did initiate the papers
309 idea, supervised the research and reviewed the manuscript. DQ discussed orbital mechanics aspects and
310 reviewed the manuscript.

FUNDING

311 This research was conducted without any institutional funding. Publication fees are covered by the
312 publication fund of the German Aerospace Center (DLR) in support for open access publishing.

DATA AVAILABILITY STATEMENT

313 This work is providing open source on all processing steps performed in the corresponding Python
314 Notebooks along with all resources in full resolution in the papers [Git-Repository](#).

REFERENCES

- 315 [Dataset] David E. Smith (2015). 2009 lunar orbiter laser altimeter radiometry data set, lro-l-lola-3-radrr-
316 v1.0. doi:10.17189/1520639
- 317 [Dataset] Ernie Wright and Noah Petro (2019). SVS: CGI Moon Kit — svs.gsfc.nasa.gov. <https://svs.gsfc.nasa.gov/4720>. [Accessed 29-07-2023]
- 318 [Dataset] European Space Agency (2023). Argonaut - technical details. https://www.esa.int/Science_Exploration/Human_and_Robotic_Exploration/Exploration/Argonaut. [Accessed 08-09-2023]
- 319 Guerrero-Gonzalez, F. J. and Zabel, P. (2023). System analysis of an ISRU production plant: Extraction of
320 metals and oxygen from lunar regolith. *Acta Astronautica* 203, 187–201. doi:10.1016/j.actaastro.2022.
321 11.050
- 322 Kornuta, D., Abbud-Madrid, A., Atkinson, J., Barr, J., Barnhard, G., Bienhoff, D., et al. (2019). Commercial
323 lunar propellant architecture: A collaborative study of lunar propellant production. *REACH* 13, 100026.
324 doi:<https://doi.org/10.1016/j.reach.2019.100026>
- 325 Lee, D. E. (2019). White paper: Gateway destination orbit model: A continuous 15 year nrho reference
326 trajectory (National Aeronautics and Space Administration (NASA)). Tech. Rep. Document ID:
327 20190030294
- 328 May, Z. D., Qu, M., and Merrill, R. (2020). Enabling global lunar access for human landing systems
329 staged at earth-moon l2 southern near rectilinear halo and butterfly orbits. In *AIAA Scitech 2020 Forum*
330 (American Institute of Aeronautics and Astronautics). doi:10.2514/6.2020-0962
- 331 Nelson, D. M., Koeber, S. D., Daud, K., Robinson, M. S., Watters, T. R., Banks, M. E., et al. (2014).
332 Mapping lunar maria extents and lobate scarps using lroc image products. *Lunar Planet. Sci.* 45, 2861
- 333 Papike, J. J., Simon, S. B., and Laul, J. C. (1982). The lunar regolith: Chemistry, mineralogy, and petrology.
334 *Reviews of Geophysics* 20, 761–826. doi:<https://doi.org/10.1029/RG020i004p00761>
- 335 Perrin, T. M. and Casler, J. G. (2016). Architecture study for a fuel depot supplied from lunar resources. In
336 *AIAA SPACE 2016* (American Institute of Aeronautics and Astronautics). doi:10.2514/6.2016-5306
- 337 Sargeant, H., Abernethy, F., Barber, S., Wright, I., Anand, M., Sheridan, S., et al. (2020). Hydrogen
338 reduction of ilmenite: Towards an in situ resource utilization demonstration on the surface of the moon.
339 *Planetary and Space Science* 180, 104751. doi:<https://doi.org/10.1016/j.pss.2019.104751>
- 340 Sato, H., Robinson, M. S., Lawrence, S. J., Denevi, B. W., Hapke, B., Jolliff, B. L., et al. (2017). Lunar
341 mare tio 2 abundances estimated from uv/vis reflectance. *Icarus* 296, 216–238. doi:10.1016/j.icarus.
342 2017.06.013
- 343 Trofimov, S., Shirobokov, M., Tselousova, A., and Ovchinnikov, M. (2020). Transfers from near-
344 rectilinear halo orbits to low-perilune orbits and the moon’s surface. *Acta Astronautica* 167, 260–271.
345 doi:10.1016/j.actaastro.2019.10.049
- 346 Whitley, R., Davis, D., Burke, L., McCarthy, B., Power, R., McGuire, M., et al. (2018). Earth-moon near
347 rectilinear halo and butterfly orbits for lunar surface exploration